

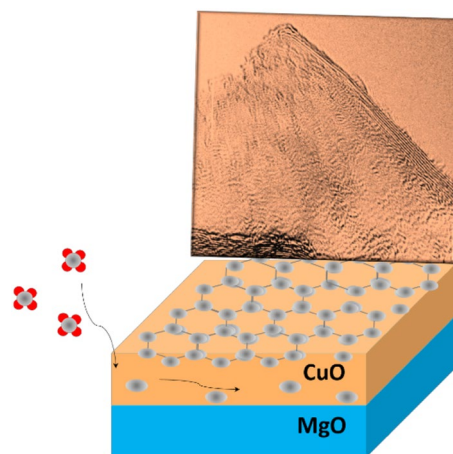
Direct Chemical Vapor Deposition Growth of Graphene Nanosheets on Supported Copper Oxide

Sebastian Dayou¹ · Brigitte Vigolo²  · Jaafar Ghanbaja² · Ghouti Medjahdi² · Mohd Zharif Ahmad Thirmizir³ · Hariy Pauzi³ · Abdul Rahman Mohamed¹

Received: 3 May 2017 / Accepted: 16 June 2017 / Published online: 28 June 2017
© Springer Science+Business Media, LLC 2017

Abstract A facile chemical vapor deposition method was used to grow multi-layer graphene. A copper-based catalyst was homogeneously deposited on magnesium oxide powder surface by impregnation. The synthesis was conducted under atmospheric pressure without a dedicated reduction step prior to the reaction. The mechanism of multi-layer graphene growth was investigated by high-resolution transmission electron microscopy, X-ray diffraction and X-ray photoelectron spectroscopy. For the first time, we show that copper under its oxide form could catalyze the growth of multi-layer graphene. Such a simple method leading to produce multi-layer graphene of quite high structural quality could help to develop alternative ways for graphene production by chemical vapor deposition.

Graphical Abstract



Keywords Chemical vapor deposition · Graphene · Catalyst · Particles

Electronic supplementary material The online version of this article (doi:10.1007/s10562-017-2125-2) contains supplementary material, which is available to authorized users.

✉ Brigitte Vigolo
brigitte.vigolo@univ-lorraine.fr

- ¹ School of Chemical Engineering, Universiti Sains Malaysia, Engineering Campus, Seberang Perai Selatan, 14300 Nibong Tebal, Pulau Pinang, Malaysia
- ² Institut Jean Lamour, CNRS-Université de Lorraine, Bd des Aiguillettes, BP 70239, 54506 Vandoeuvre-Lès-Nancy, France
- ³ Science and Engineering Research Center, Universiti Sains Malaysia, Engineering Campus, Seberang Perai Selatan, 14300 Nibong Tebal, Pulau Pinang, Malaysia

1 Introduction

Graphene has generated a huge interest within the scientific community due to its unique physical properties that have not been previously observed in nano-scale [1]. This allows graphene to be applied in myriad applications including, but not limited to, flexible electronics [2], sensors and biosensors [3, 4], bioengineering [5], biomedical [6], composite materials [7], energy technology [7, 8] and solar cells [9]. Chemical vapor deposition (CVD) methods have been reported as the most popular route for wafer-scale graphene production [10] but it can also be used to synthesize graphene nanosheet [11–13], typically on metal nanoparticles. The low carbon solubility in copper has led it to become

the most used catalyst for the synthesis of graphene by CVD due to a surface-mediated growth mechanism [14].

Current CVD methods require multiple steps for graphene growth. Prior to the CVD growth stage, a reduction stage is commonly applied. It often involves a hydrogen pretreatment at high temperature to remove the native oxides and restore the metal character of the catalyst surface. This is due to the commonly held belief about the low catalytic activity of metal oxide for graphene growth [15]. It has been shown that the presence of oxygen on the surface of copper significantly reduces the graphene nucleation density by passivating the active sites for graphene growth [16]. It was even reported that a copper oxide layer is catalytically inactive for graphene growth [17]. However, in a recent study, Gottardi et al. demonstrated the ability to grow graphene on copper oxide foil [18]. Moreover, their work shows that graphene grown by copper oxide displays comparable electronic band structure and properties as freestanding graphene. This finding is leading to change course regarding the ability of metal oxide to grow graphene by CVD and it is even more clearly an open question. And this approach also prompts the question if a dedicated reduction stage prior to CVD growth is necessary. It is furthermore favorable to simplify the graphene growth processes by avoiding multiple approaches; the subsequent reduced production cost could help in promoting commercialization of graphene [19].

Magnesium oxide (MgO) is commonly used in thermal-related applications because it exhibits good thermal stability and conductivity. However, in certain applications such as thermal energy storage, the thermal conductivity of MgO alone does not fulfill the requirements for rapid heat charge and discharge, thus addition of thermal conductivity enhancer is necessary [20–22] and graphene is an ideal filler due to its superior thermal conductivity properties [23]. Moreover, direct growth of graphene nanosheets on copper–MgO surface may provide a solution to the dispersion issue in composites prepared by a conventional mixing process [21, 24]. MgO is a well-known support material for metal catalyst for the CVD growth of various carbon nanostructures including carbon nanotubes (CNTs) [25–27] and graphene materials [28].

In the present work, we show that graphene nanosheets could be grown on copper oxide by using a simple CVD growth method. Copper used as catalyst was deposited on MgO powder by impregnation and the graphene growth was conducted without a dedicated reduction stage prior to the CVD reaction. The mechanism by which graphene grows on copper oxide in this single-stage process was investigated. MgO here acts as dispersing agent and we show that copper oxide particles are homogeneously deposited on MgO surface. Copper-based particles protected by graphene layers could be deeply studied and analyzed by

X-ray diffraction (XRD) and X-ray photoelectron spectroscopy (XPS). The oxidation degree of copper depending on the different operating conditions used for the CVD reaction was, especially, studied. This novel composite has the potential to be the next-generation material to exploit the expected enhanced thermal conductivity for thermal energy storage applications.

2 Experimental Section

2.1 Catalyst Preparation and CVD Growth

Cu–MgO was prepared by impregnation of MgO with an ethanol solution of copper(II) chloride. MgO (HmbG Chemicals) (10 g) were mixed into an ethanol solution of CuCl_2 (Acros) (50 mL) under stirring and then sonicated for 60 min. After being evaporated to dryness at 85 °C, the solid was baked at 130 °C for 12 h and then ground into fine powder. Subsequently, the powder was calcined at 950 °C for 3 h before being used to catalyze the deposition of graphene. To verify the effective deposition of Cu on MgO, X-ray fluorescence (XRF) analysis was performed on the as-prepared Cu–MgO sample and compared with raw MgO. From XRF, the content of copper is around 7 wt% in the prepared catalyst in agreement with the starting concentration of CuCl_2 . The XRF results also revealed the presence of iron in low content (around 0.3 wt%) in the raw MgO powder.

For the CVD process, naked calcined MgO or the prepared Cu–MgO catalyst powder (0.25 g) was distributed uniformly over a quartz boat and inserted into the middle of a quartz tube. The furnace was slowly heated under N_2 atmosphere (100 mL/min) until it reached the desired temperature (950, 980 or 1000 °C). Hydrogen and methane (2:1 volumetric ratio) were then introduced into the furnace (at 150 mL/min) for a reaction time from 10 to 60 min. After the chosen growth time, the system was allowed to naturally cool down to room temperature under N_2 gas. Dissolution of MgO was done in nitric acid (2 M) at room temperature under stirring for 30 min. The harvested powder was then washed with de-ionized water under filtration on a polyvinylidene fluoride membrane (0.22 μm of porosity) and dried in oven (around 100 °C) before being heated at 500 °C for 60 min.

2.2 Characterization Techniques

Chemical analysis of the samples was performed by XRF using a Bruker AXS S4 Explorer wavelength-dispersive spectrometer. Transmission electron microscopy (TEM) was performed using a JEOL ARM 200F cold FEG and a FEI Tecnai G2 F20 S-TWIN with field emission apparatus

at an operating voltage of 80 and 200 kV, respectively. Before observation, the powder was dispersed in ethanol in a low-power sonication bath for a few minutes and deposited on a holey carbon grid (200 mesh size). Selected area electron diffraction (SAED) was also performed on chosen areas. Scanning electron microscopy (SEM) observations were carried out using an XL30 S-FEG apparatus using an ultra high resolution (UHR) mode and FEI Verios 460L apparatus using an extreme high resolution with field emission. The latter is equipped with energy dispersive X-ray spectrometer using Oxford X-Max Silicon Drift Detector for elemental mapping analysis to investigate the homogeneity of copper deposition on the surface of MgO particles after the catalyst is prepared. XPS analysis was done using a Kratos AXIS Ultra DLD equipped with a monochromatic $Al_{K\alpha}$ X-ray source (1486.6 eV). Core level spectra were recorded under hybrid lens mode with slot aperture and the pass energy of the hemispherical analyzer was set at 20 eV. XRD data were recorded using a X'Pert PRO MPD (multi purpose diffractometer) system with a copper ($Cu\ K\alpha$) radiation ($\lambda = 1.54056 \text{ \AA}$) and X'celerator as detector. The powder was placed on a silicon zero-background sample holder with a hole of a 1 mm-depth. For each sample, the hole is filled with the powder in the same manner keeping relatively constant the analyzed volume. Diffraction data were collected between 10° and 100° (2θ). Raman spectra of the as-synthesized product after CVD were measured with a Renishaw inVia Raman microscope using an excitation line of 632.8 nm argon laser.

3 Results and Discussion

3.1 Growth of Graphene Materials

Particles of 10–100 nm in diameter well-dispersed on MgO surface are noticeable from SEM observations (Fig. 1a). EDS mapping shows that copper element was homogeneously deposited on MgO powder by the applied impregnation method (Fig. 1b). After our one-step synthesis method, occurrence of few-layer graphene (FLG) or multi-layer graphene (MLG) growth was directly verified by TEM and SEM observations on sample after MgO solubilization. MgO solubilization was conducted to better visualize the graphene morphology especially under SEM whereby the presence of MgO can produce charging effect that would hinder a high quality imaging. The structural characteristics of the carbon nanomaterials were carefully investigated by high-resolution (HR) TEM. SEM and TEM observations revealed the presence of graphene materials for the samples produced by CVD at 950°C for 60 min, 980°C for 30 min and 1000°C for 30 min, no graphene layers were found for the synthesis done at 950°C for 30 min. The

grown graphene nanosheets appear under two forms: crumpled organization flower petal-like shape and a platelet-like structure (Fig. 2a, c for the sample prepared at 950°C for 60 min and Fig. 2b, d for the sample grown at 1000°C for 30 min). The crumpled form is reported to result from agglomeration of graphene nanosheets that naturally curve [29]. In both samples, the flower-like form of graphene is the shape mainly observed.

Typical TEM images of graphene nanosheets obtained after CVD synthesis done at 950°C for 60 min, 980°C for 30 min and 1000°C for 30 min are shown in Fig. 3a–f, respectively. The as-produced graphene is well separated from the surface from which it was grown certainly due to sonication used for the sample preparation for TEM analyses. Based on the observations between the graphene samples produced, all the graphene features observed under SEM (and also TEM) are rather similar for the different CVD conditions used. Observations under HRTEM clearly revealed thin graphene nanosheets with wrinkles and ripples commonly observed features on thin MLG or FLG. Bending of the grown graphene nanosheets is certainly facilitated by their weak thickness of a maximum of ten layers (Fig. 4a) and more often around two to five layers (Fig. 4b, c). The variation in the number of layers observed here is currently encountered for a CVD grown graphene on metal particles [11–13]. It could be due to the variation in size of copper nanoparticles in the prepared catalyst. This is in contrast to the highly uniform number of layers that can be obtained for wafer-scale graphene grown on metallic copper foils [30]. The graphene nanosheets produced in this work were relatively thin in comparison with the grown graphene using metallic copper powder [31].

Electron diffraction was systematically done on the observed zones to check the characteristic interlayer distances. One must be cautious regarding the aspect of graphene grown on MgO since MgO itself can appear with similar shapes than those reported for graphene, i.e. thin platelets [29, 32, 33]. This is the reason why SAED analysis was used to confirm the graphitic structure of the grown graphene nanosheets. Figure 5 shows a typical two-dimensional electronic diffraction image acquired with diffraction positions at $d = 0.335 \text{ nm}$ and $d = 0.203 \text{ nm}$ from the reflections (002) and (101); they confirm the graphitic order of the synthesized MLG in all samples. The low signal of the electronic diffraction from the grown MLG is expected due to its very low thickness (Fig. 4).

A flat graphene morphology that possesses periodic stacking typically produces electronic diffraction in spot pattern. However, in our sample, the diffraction patterns appear as rings due to graphene sheet stacking disorder, as manifested by the crumpled morphology, resulting in many graphitic orientations (Fig. 5a), akin to a turbostratic structure [34]. Addition of all spots originated from each of

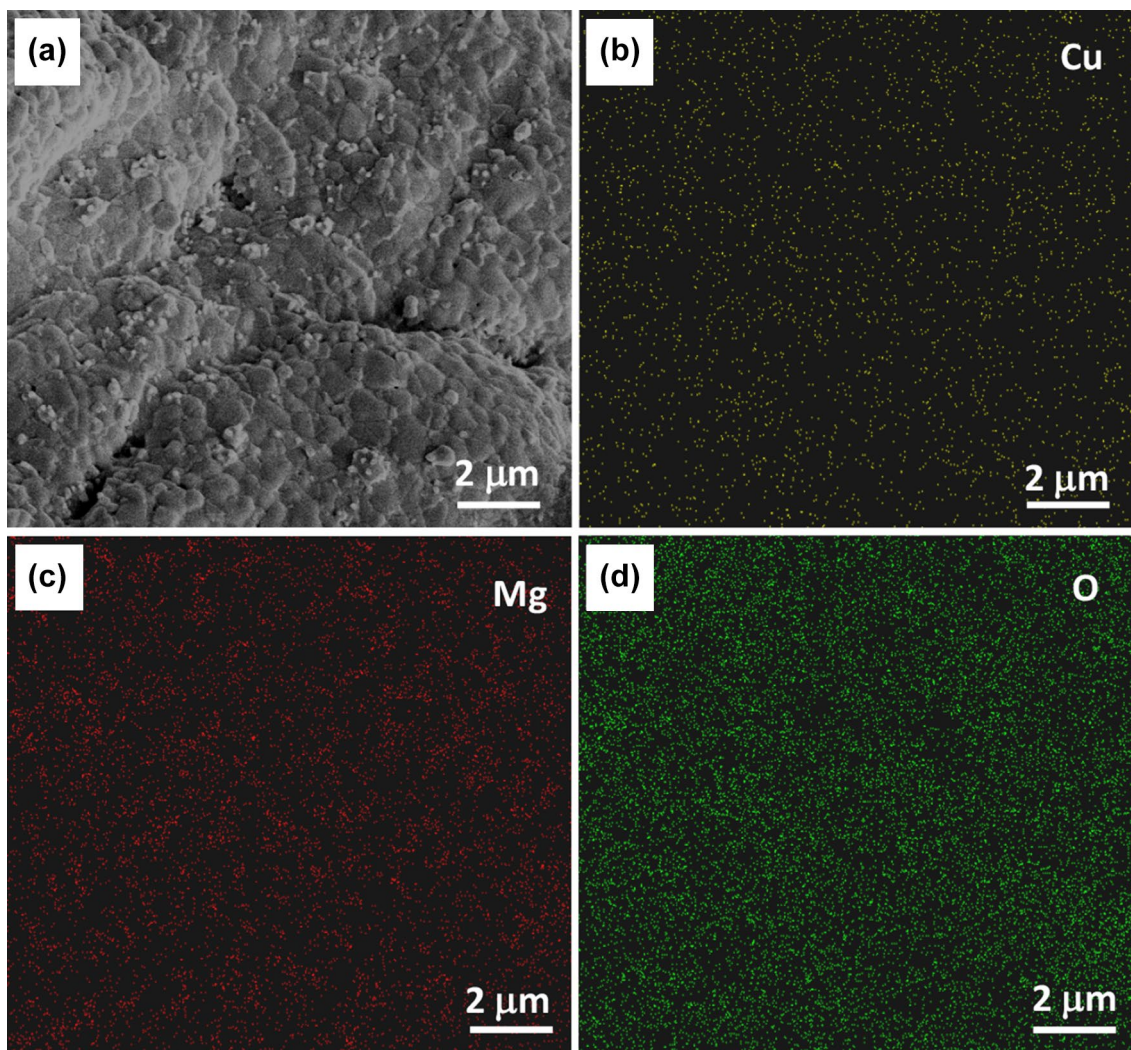


Fig. 1 X-ray mapping of 5% Cu–MgO: **a** SEM image, **b** Cu map, **c** Mg map, **d** O map

these graphene sheets, hence, builds continuous ring. It is important to note that a broad single halo instead of periodic rings are characteristics of amorphous carbon which is absent in our sample in agreement with detailed observations done by TEM. The visualization of several diffraction rings by SAED on a window of tens of nanometers only, is the sign of a high structural quality of the grown graphene in all samples.

Although the material produced is predominantly graphene, the presence of single-walled nanotubes (SWNTs) and multi-walled CNTs (MWNTs) could be rarely noticed by TEM after solubilization of MgO. The growth of these CNTs can be attributed to Fe impurities present in the used commercial MgO. This is further attested from investigations on CVD growth on MgO without addition of Cu

which clearly shows that SWNTs and MWNTs could be grown on copper-free MgO. Because of Raman resonance of these CNTs which dominates the signal, Raman spectroscopy could not be used here to characterize the produced MLG.

3.2 Growth Mechanism

The mechanism of graphene growth catalyzed by copper particles deposited on MgO by CVD is not known yet. In particular, copper is obviously not under its metal form during the growth stage as it is usually the case for conventional CVD reactions with metallic copper foils [15, 35]. The oxidation state of copper is an important parameter to identify the species of copper during the growth stage

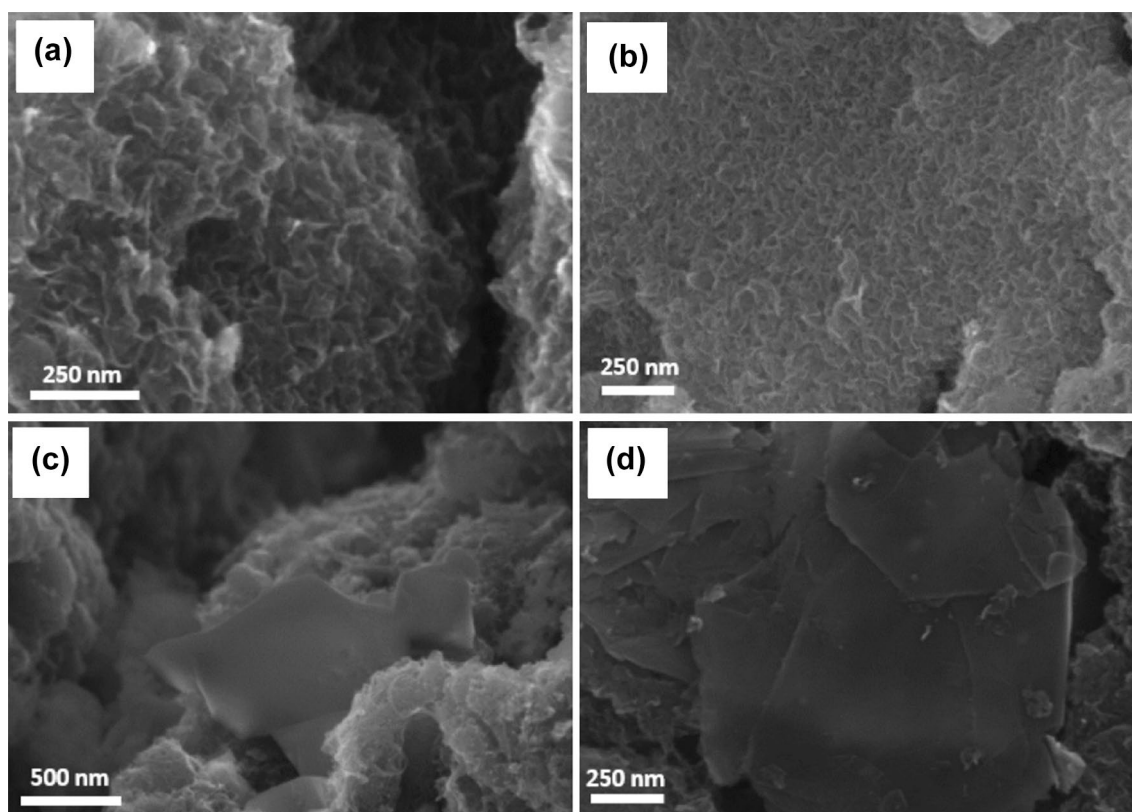


Fig. 2 Typical UHR SEM images showing the two forms of MLG after the CVD synthesis done at 950 °C, 60 min (**a**, **c**), 1000 °C, 30 min (**b**, **d**) and after solubilization of MgO

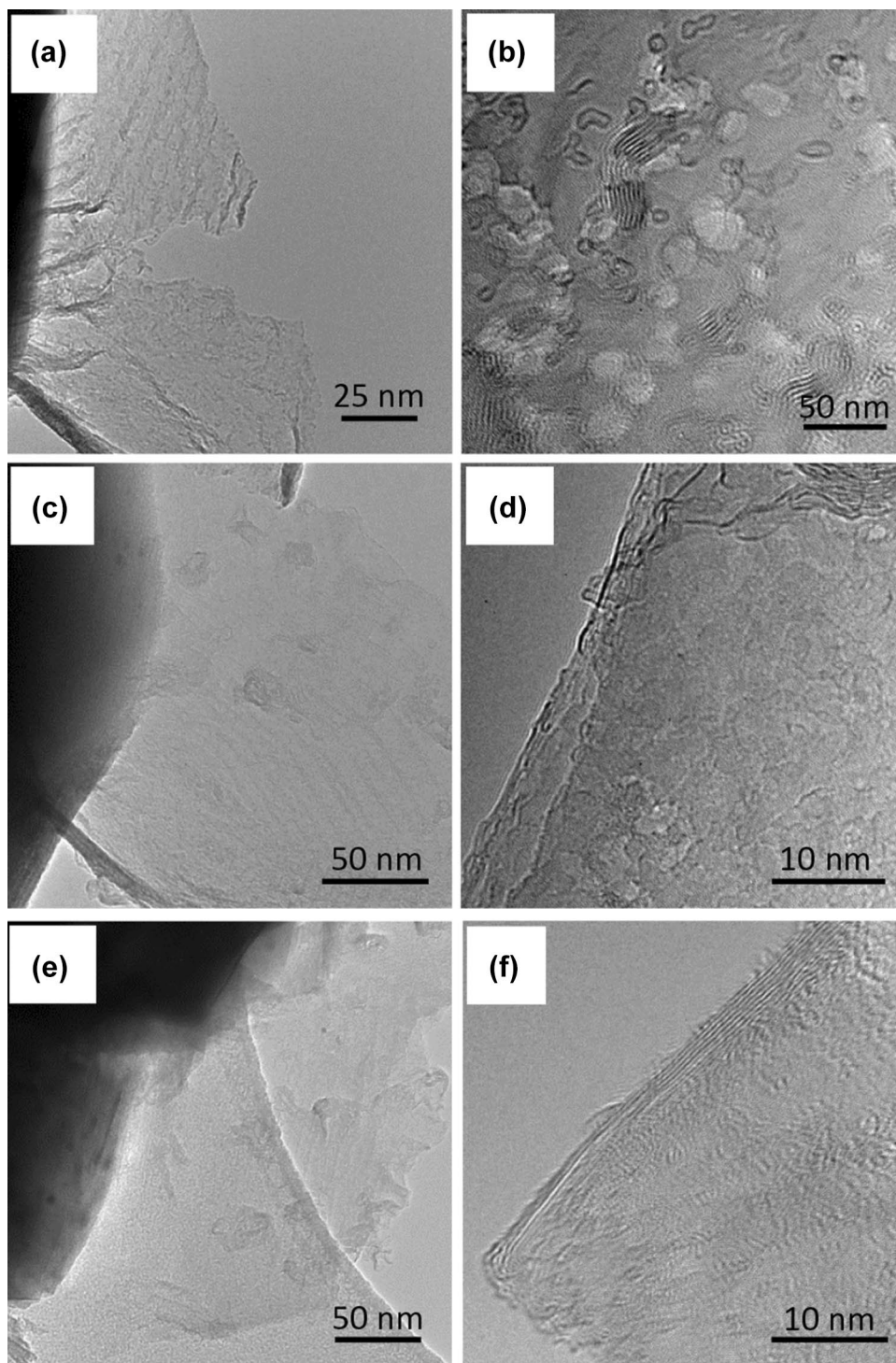
within the synthesis chamber. Locally, TEM observations focused on copper particles (Fig. 6), especially on encapsulated copper particles for which the oxidation state is expected to be preserved after the CVD reaction [36, 37].

For a more global analysis, XRD and XPS analyses were performed before and after the CVD reaction. XRD patterns show that presence of CuO is obvious for all the conditions and a reduction reaction of CuO seems to take place as either CVD time or temperature is increased (Fig. 7). Diffraction peaks of Cu₂O and also Cu are more pronounced for the sample prepared at 980 and 1000 °C for 30 min. The XRD data also gives additional evidence of the presence of graphitic materials in the post-CVD samples especially visible for the sample prepared at 1000 °C for 30 min. The peak at around 26° could be indeed indexed to the (002) plane of a typical graphite structure. A broad shape of this diffraction peak is expected due to the weak number of layers for the produced MLG. The peak at around 18.5° corresponds to (001) plane of Mg(OH)₂ (hexagonal phase of lattice parameters $a=3.147$ and $c=4.769$) in the samples after CVD which is formed due to hydration of MgO at ambient conditions.

The XPS core level spectrum in the Cu 2p energy region shows the two main satellite peaks of Cu 2p_{3/2} (933 eV) and Cu 2p_{1/2} (953 eV) and their respective shake-up satellite peaks observed at 941 and 960 eV [38]. These shake-up satellite peaks are characteristic of a Cu^{+II} state certainly belonging to CuO. The shake-up satellite peaks are observed in the Cu–MgO prepared catalyst and also in the post-CVD samples but with lower intensity compared with the former one which denoted a less amount of CuO after the CVD reaction (Fig. 8a). In agreement with Cu binding energy, the core level XPS spectrum in the O 1s energy region shows an upshift that corresponds to an increased amount of Cu₂O after CVD (Fig. 8b). It should be noted, however, that it is insufficient to distinguish between copper metal (Cu⁰) and Cu^{+I} in Cu₂O from the Cu 2p energy region since their peaks at binding energy Cu 2p_{3/2} and Cu 2p_{1/2} are almost the same [39]. C 1s spectra are in complete agreement with a carbon sp² conjugated network as expected for graphene (cf. Supporting Information).

It has been shown that CuO is easily formed on the surface of MgO by calcination at high temperature under air [40, 41]. Although the prepared catalyst, i.e.

Fig. 3 Typical TEM and HRTEM images of graphene after the CVD synthesis done at 950 °C for 60 min (**a, b**), 980 °C for 30 min (**c, d**) and 1000 °C for 30 min (**e, f**)



CuO–MgO does not undergo any reduction stage prior to the CVD reaction, a reduction reaction can be induced during the reaction stage by either the hydrogen present in the gas mixture during the CVD reaction or carbon atoms from methane via a carboreduction phenomenon.

In this study, CuO would be reduced mainly by hydrogen gas, which is known to have higher reducing power than that of methane [42], especially in the beginning part of the reaction process as the carbon atoms from methane was consumed for CNT formation by Fe

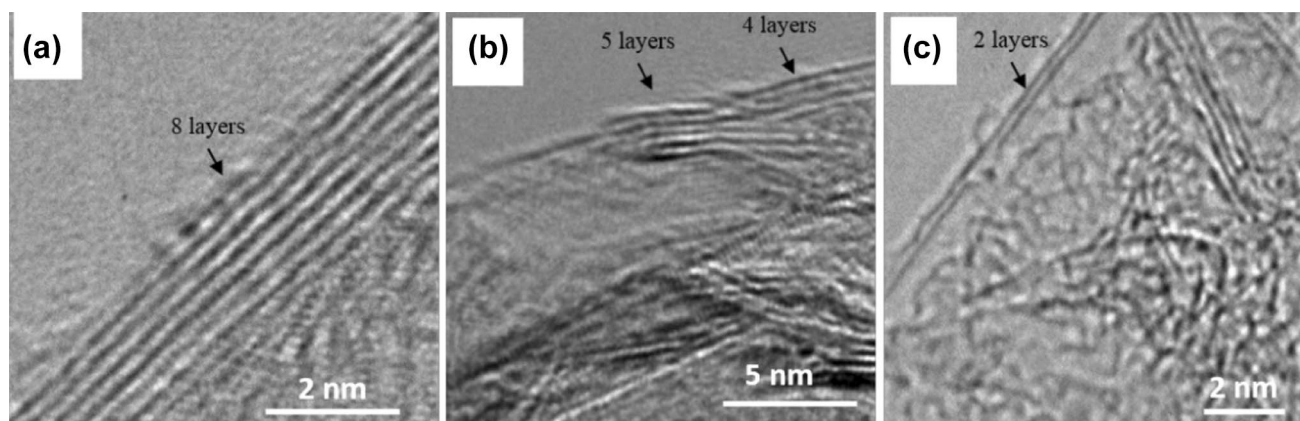


Fig. 4 Typical HRTEM images focused on the edges of FLG and MLG for the commonly encountered graphene in the prepared samples

Fig. 5 TEM micrograph of the graphenic material (a) and corresponding SAED pattern (b); reflections (002) and (101) from the graphitic-ordered structure of the grown multi-layer MLG correspond to $d_{002} = 0.335$ nm and $d_{101} = 0.203$ nm

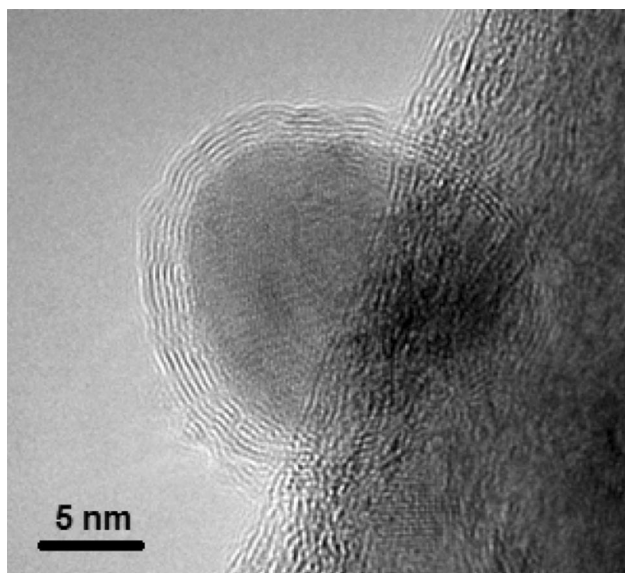
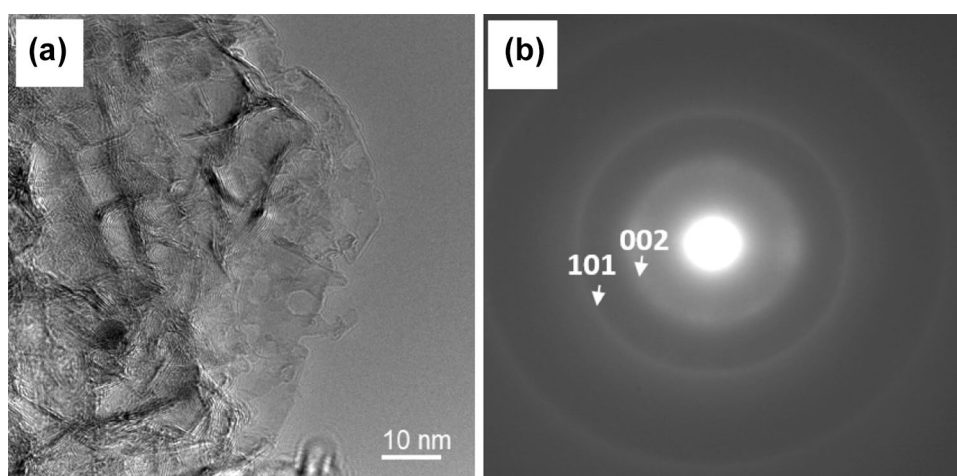


Fig. 6 TEM micrograph of an encapsulated copper-based particle at the surface of MgO (CVD reaction done at 950 °C for 60 min)

impurities. Phenomenological models, i.e. the nucleation/growth model or the interface model, have often been used to explain the reduction mechanism of metal oxides [43–46]. Both models describe that the reduction process is followed by the creation of oxygen vacancies on the surface. This type of defect is reactive, thus provides sites for methane dehydrogenation to occur at the intermediate stage of the reaction, before the construction of graphitic network to form graphene layer [18]. The schematic representation of the growth mechanism of graphene layers in our process is shown in Fig. 9. We speculate that the reduction process could continue to occur internally [44] after MLG was formed on the surface of copper species, as oxygen atoms from the bulk diffuse out to fill the vacant spots on the CuO surface that would result in a reduced copper species (either Cu_2O or Cu) in the core of the CuO particles. The fact that CuO phase is still present even after CVD completion shows that CuO did not undergo a complete reduction. A partial reduction of CuO to Cu_2O and a small part can be reduced even to

Fig. 7 XRD patterns before (substrate after calcination) and after the CVD reaction done at different conditions: at 950 °C for 30 and 60 min, at 980 °C for 30 min and at 1000 °C for 30 min. Assignment of the diffraction peaks: *red* for MgO, *green* for CuO, *orange* for Cu₂O and *blue* for Cu. The *stars* identify the peaks that have not been assigned. Cu K α radiation at $\lambda = 1.54056 \text{ \AA}$

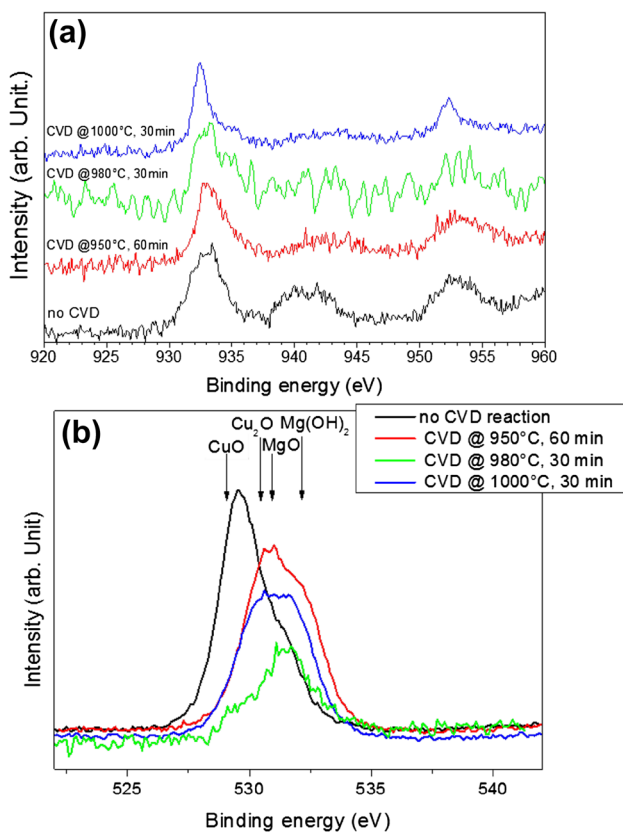
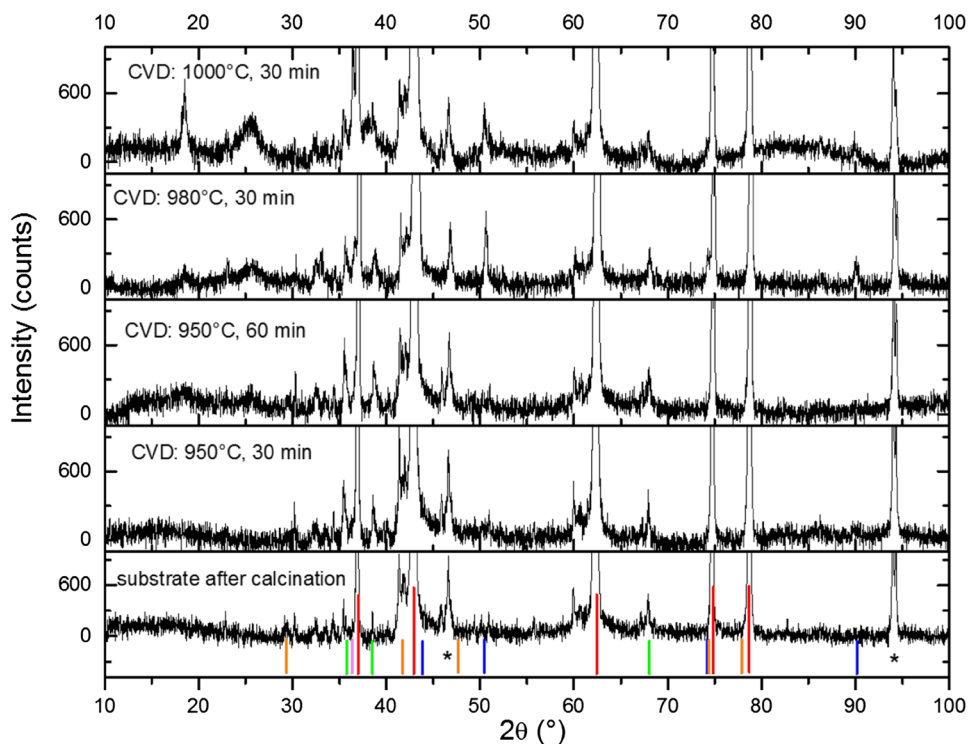


Fig. 8 XPS spectra of Cu 2p (a) and O 1s (b) of the Cu–MgO prepared catalyst and samples after the CVD reaction done at 950 °C for 60 min, at 980 °C for 30 min and at 1000 °C for 30 min

Cu for the highest temperatures used since oxygen vacancies can be easily created at elevated temperature. Copper mainly remains as copper oxide during the formation of graphene nanosheets by our CVD method. Certainly, the presence of oxide favors the formation of graphene material, instead of CNTs as it is usually the case for pure copper metal nanoparticles [47, 48].

4 Conclusion

The growth of graphene nanosheets was performed by means of a straightforward CVD method. The catalyst was prepared by a wet impregnation of a commercial MgO powder by copper chloride. No dedicated reduction stage was used prior to the CVD reaction although reduction process did occur during the reaction stage due to presence of hydrogen in the gas mixture. The CVD reaction was conducted under atmospheric pressure with methane as the carbon source. We have unambiguously identified the oxidation state of copper by XRD and XPS. And we have produced the experimental proof that multi-layer graphene was able to grow on copper oxide. Our method is also of great interest because it is a simple process that could dramatically reduce the production cost of graphene nanosheets. Moreover, the as-produced material is a MgO/graphene composite that could be directly exploited for its thermal properties.

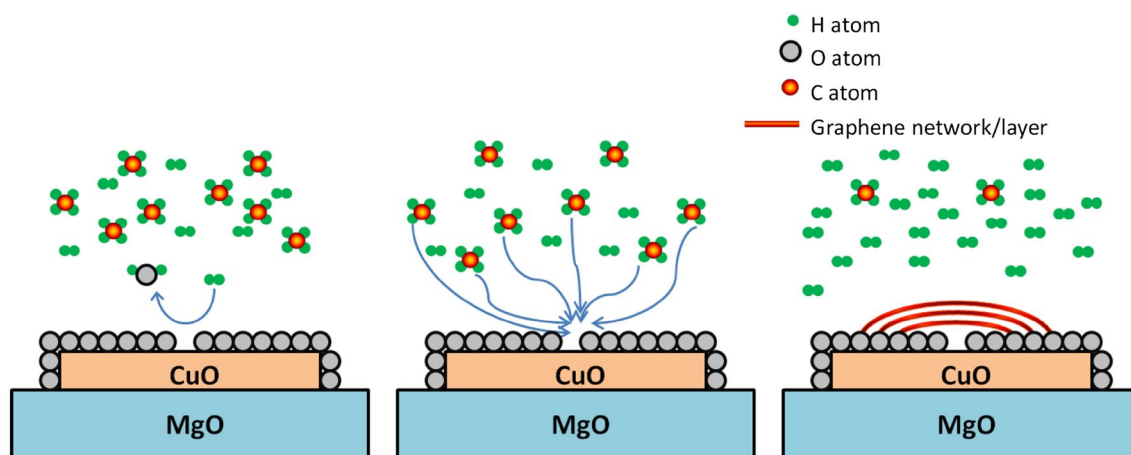


Fig. 9 Graphene growth mechanism. Creation of oxygen vacancy due to reduction phenomenon by hydrogen. At these defective sites, favored dehydrogenation of methane gases. Facile formation of graphene layers

Acknowledgements The authors thank L. Garoux for the XRF measurements. The authors gratefully acknowledge the financial support provided by the IReC Grant (1002/PJKIMIA/910404) and Science Fund Grant (Project No. 03-01-05-SF0659).

References

- Geim AK, Novoselov KS (2007) *Nat Mater* 6:183
- Novoselov KS, Fal'ko VI, Colombo L, Gellert PR, Schwab MG, Kim K (2012) *Nature* 490:192
- Liu J, Liu Z, Barrow CJ, Yang W (2015) *Anal Chim Acta* 859:1
- Green NS, Norton ML (2015) *Anal Chim Acta* 853:127
- Gao H, Duan H (2015) *Biosens Bioelectron* 65:404
- Krishna KV, Ménard-Moyon C, Verma S, Bianco A (2013) *Nanomedicine* 8:1669
- Wang Z, Liu C-J (2015) *Nano Energy* 11:277
- Hu C, Song L, Zhang Z, Chen N, Feng Z, Qu L (2015) *Energy Environ Sci* 8:31
- Das S, Sudhagar P, Kang YS, Choi W (2014) *J Mater Res* 29:299
- Hofmann S, Braeuninger-Weimer P, Weatherup RS (2015) *J Phys Chem Lett* 6:2714
- Chen Z, Ren W, Liu B, Gao L, Pei S, Wu Z-S, Zhao J, Cheng H-M (2010) *Carbon* 48:3543
- Shan C, Tang H, Wong T, He L, Lee ST (2012) *Adv Mater* 24:2491
- Shen Y, Lua AC (2013) *Sci Rep* 3:3037
- Li X, Cai W, An J, Kim S, Nah J, Yang D, Piner R, Velamakanni A, Jung I, Tutuc E, Banerjee SK, Colombo L, Ruoff RS (2009) *Science* 324:1312
- Mattevi C, Kim H, Chhowalla M (2011) *J Mater Chem* 21:3324
- Hao Y, Bharathi MS, Wang L, Liu Y, Chen H, Nie S, Wang X, Chou H, Tan C, Fallahzad B, Ramanarayan H, Magnuson CW, Tutuc E, Yakobson BI, McCarty KF, Zhang Y-W, Kim P, Hone J, Colombo L, Ruoff RS (2013) *Science* 342:720
- Zhou H, Yu WJ, Liu L, Cheng R, Chen Y, Huang X, Liu Y, Wang Y, Huang Y, Duan X (2013) *Nat Commun* 4:2096
- Gottardi S, Müller K, Bignardi L, Moreno-López JC, Pham TA, Ivashenko O, Yablonskikh M, Barinov A, Björk J, Rudolf P, Stöhr M (2015) *Nano Lett* 15:917
- Zurutuza A, Marinelli C (2014) *Nat Nano* 9:730
- Ye F, Ge Z, Ding Y, Yang J (2014) *Particuology* 15:56
- Ge Z, Ye F, Ding Y (2014) *ChemSusChem* 7:1318
- Ge Z, Li Y, Li D, Sun Z, Jin Y, Liu C, Li C, Leng G, Ding Y (2014) *Particuology* 15:2
- Balandin AA (2011) *Nat Mater* 10:569
- Ge Z, Ye F, Cao H, Leng G, Qin Y, Ding Y (2014) *Particuology* 15:77
- Lin M, Ying Tan JP, Boothroyd C, Loh KP, Tok ES, Foo Y-L (2006) *Nano Lett* 6:449
- Xiong G-Y, Wang DZ, Ren ZF (2006) *Carbon* 44:969
- He M, Liu B, Chernov AI, Obratsova ED, Kauppi I, Jiang H, Anoshkin I, Cavalca F, Hansen TW, Wagner JB, Nasibulin AG, Kauppinen EI, Linnekoski J, Niemelä M, Lehtonen J (2012) *Chem Mater* 24:1796
- Wang X, You H, Liu F, Li M, Wan L, Li S, Li Q, Xu Y, Tian R, Yu Z, Xiang D, Cheng J (2009) *Chem Vap Depos* 15:53
- Wang G, Shen X, Yao J, Park J (2009) *Carbon* 47:2049
- Lee K, Ye J (2016) *Carbon* 100:441
- Koltsova TS, Nasibulina LI, Anoshkin IV, Mishin VV, Kauppinen EI, Tolochko OV, Nasibulin AG (2012) *J Mater Sci Eng B* 2:240
- Wang H, Sun X, Liu Z, Lei Z (2014) *Nanoscale* 6:6577
- Baumann SO, Schneider J, Sternig A, Thomele D, Stankic S, Berger T, Grönbeck H, Diwald O (2015) *Langmuir* 31:2770
- Monthieux M, Noé L, Kobylko M, Wang Y, Cazares-Huerta TC, Pénicaud A (2017) *Carbon* 115:128
- Kalbac M, Frank O, Kavan L (2012) *Carbon* 50:3682
- Chen S, Brown L, Levendorf M, Cai W, Ju S-Y, Edgeworth J, Li X, Magnuson CW, Velamakanni A, Piner RD, Kang J, Park J, Ruoff RS (2011) *ACS Nano* 5:1321
- Shi L, Wang R, Zhai H, Liu Y, Gao L, Sun J (2015) *PCCP* 17:4231
- Fleisch TH, Mains GJ (1982) *Appl Surf Sci* 10:51
- Marella RK, Koppadi KS, Jyothi Y, Rama Rao KS, Burri DR (2013) *New J Chem* 37:3229
- El-Molla SA (2006) *Appl Catal A* 298:103
- Nagaraja BM, Padmasri AH, Raju BD, Rama Rao KS (2011) *Int J Hydrogen Energy* 36:3417
- Artizzu P, Garbowski E, Primet M, Brulle Y, Saint-Just J (1999) *Catal Today* 47:83
- Rodríguez JA, Hanson JC, Frenkel AI, Kim JY, Pérez M (2002) *J Am Chem Soc* 124:346
- Yuan L, Van Der Geest AG, Zhu W, Yin Q, Li L, Kolmogorov AN, Zhou G (2014) *RSC Adv* 4:30259

45. Furstenuau RP, McDougall G, Langell MA (1985) *Surf Sci* 150:55
46. Ressler T, Jentoft RE, Wienold J, Günter MM, Timpe O (2000) *J Phys Chem B* 104:6360
47. Lin J-H, Chen C-S, Zeng Z-Y, Chang C-W, Chen H-W (2012) *Nanoscale* 4:4757
48. Zhou W, Han Z, Wang J, Zhang Y, Jin Z, Sun X, Zhang Y, Yan C, Li Y (2006) *Nano Lett* 6:2987